

# Spin crossover dynamics from first principles: Effects of ligand substitution and solvent environment.

Huiwen Tan, Nadeem Natt, and Benjamin J. Powell\*

*School of Mathematics and Physics, The University of Queensland, Brisbane, Queensland,  
4072, Australia*

E-mail: [powell@physics.uq.edu.au](mailto:powell@physics.uq.edu.au)

## Abstract

Spin crossover dynamics in phosphorene complexes  $[\text{Fe}(\text{dppen})_2\text{X}_2]$  ( $X = \text{Br}$  and  $\text{Cl}$ ) is investigated using density functional theory. Material specific first principles calculations are conducted to obtain adiabatic free energy surface and kinetic barriers describing the low spin state and high spin state interconversions, mediated by a high energy intermediate spin state. The interplay of the electronic energies, spin-orbit interaction, and molecular vibrations in determining the materials specific thermal and kinetic properties is presented. Furthermore, the influence of halogens ( $X$ ) and solvent environments (vacuum, chloroform and trichloromethane) on the spin crossover properties of the compounds is explored. Br anion in the coordination sphere slows kinetic relaxations of photo-induced trapped HS state and reduces the thermal spin crossover temperature  $T_{1/2}$  when compared to Cl. This results from a smaller energy gap between LS and HS states for Br. Calculations predict that the solvents reduce the energy gap between the LS and HS states and effect the free energy barriers, thus modifying SCO dynamics in these compounds.

# Introduction

Coordination complexes of first-row transition metals may exhibit spin crossover—interconversion between low-spin (LS) and high-spin (HS) electronic states. In Fe(II) complexes, the interconversions (total spin  $S = 0 \leftrightarrow S = 2$ ) carry large structural reorganisations, without breaking or making any bonds<sup>1</sup>. The spin crossover (SCO) can be induced by applying external perturbations, such as temperature<sup>1</sup>, pressure<sup>2,3</sup>, light<sup>4,5</sup>, and electric field<sup>6</sup>. Switching between the spin states has been proposed as a route to realise applications of spin-crossover materials in optoelectronic, spintronic, and molecular electronic devices<sup>7</sup>. An important question is how small chemical changes, such as the substitution of halogen elements in the coordination sphere and the solution environment of SCO complexes affect the bistability<sup>8,9</sup>. Computational studies to model specific spin crossover materials are required for understanding and predicting these effects.

SCO is a complex dynamic process that involves a configurational change of a large number of atomic coordinates. Transition between the spin states is spin-forbidden in  $d^6$  metal coordination complexes. Spin-orbit interaction partially relaxes this constraint via intersystem crossings between the spin states that have  $\pm 1$  difference in the total spin<sup>10,11</sup>. Thus mediation of at least one intermediate spin state<sup>10,11</sup> is required in  $d^6$  SCO complexes. SCO theories have been mainly limited to phenomenological models, that are not parameterised for specific materials.<sup>12–16</sup> Many phenomenological theories of the LS-HS transition introduce abrupt nonphysical changes in, e.g., forces and configurations. This hinders the quantum chemical modelling of SCO. Thus, DFT-based calculations of specific SCO materials have frequently been restricted to estimating the 0 K enthalpy differences between the spin states and determining structures of materials<sup>17–21</sup>. Explicit DFT modelling of the SCO dynamics requires calculations involving both the electronic and ionic degrees of freedom to determine reaction pathways and associated reaction rates. Previously, only a handful of DFT-based works have introduced computational approaches that model the SCO process for specific materials.<sup>22–24</sup> Cirera *et. al.* presented an efficient DFT-based modelling of

the SCO materials by applying a hybrid MD and MC method on the adiabatic potentials of the HS and LS states.<sup>22,23</sup> Vela *et. al.* applied DFT plus machine learning to explore full configuration space minimum energy crossing among the adiabatic free energy surfaces of LS, IS and HS and calculated the thermal and dynamics properties with remarkable accuracy.<sup>24</sup> However, a limitation of these works is that they require abrupt jumps between the potential energies of different spin states. We show below that this can be avoided by explicit consideration of the spin-orbit interaction.

Recently, a semi-empirical semi-classical model was derived from the crystal field theory for  $d^6$  transition metal complexes – showing that only one adiabatic potential energy surface with mixed LS, HS and high energy spin states describes the SCO dynamics.<sup>5</sup> The simple model considered only a single ionic coordinate from the coordination sphere. To predict the thermal and dynamic properties of specific materials, comprehensive materials calculations of the adiabatic SCO potential surface are required.

In this paper, a parameter-free first-principles approach to model the dynamic SCO processes is presented, based on insights from our semi-empirical semi-classical model.<sup>5</sup> Starting from the molecular structures in the LS and HS states, potential energy surfaces (PESs) in the LS, intermediate spin and HS spin states are calculated by density functional theory (DFT). The spin-orbit couplings between the spin states are explicitly calculated from DFT. Temperature-dependent free energy surfaces (FESs) are constructed by including the entropy and enthalpy contributions of the vibrational states. Finally we apply transition state theory (TST) to describe the spin crossover dynamics on DFT-based free energies and kinetic barriers.

As a proof-of-principle study, we present the DFT calculations of the SCO process for two phosphorene complexes. We study  $[\text{Fe}(\text{dppen})_2X_2]$  ( $1X_2$ ) in three solvent environments vacuum, trichloromethane (tcm) =  $\text{CHCl}_3$  and chloroform (dcm) =  $\text{CH}_2\text{Cl}_2$ , where dppen = *cis*-1,2-bis(diphenylphosphino)ethylene and ( $X = \{\text{Br}^{-1}, \text{Cl}^{-1}\}$ ). We investigate the effects of the halide ions and solvents on thermal and dynamic SCO properties. Key properties of

interest are thermal SCO temperature – at which half of the population is in each spin state,  $T_{1/2}$ , and a temperature characterizing kinetic bistability  $T_{\text{LIESST}}$ <sup>25,26</sup>. Experimentally, these compounds were studied in solid-state<sup>9,27–29</sup>, where strong variations of  $T_{1/2}$  and  $T_{\text{LIESST}}$  values were observed with halogen and crystal environment changes. We find a strong influence of halogen anion and of the solution environments on the enthalpy differences and free energy kinetic barriers. Thus variations in the calculated value of  $T_{1/2}$  and  $T_{\text{LIESST}}$  for different cases of halogens and solvents.

## Computational Details

All DFT calculations were performed with ADF2020<sup>30</sup> in the Amsterdam Modeling Suite (AMS).  $\text{Fe}(\text{dppen})_2\text{Br}_2$  and  $\text{Fe}(\text{dppen})_2\text{Cl}_2$ , as ferrous SCO materials, were studied herein at the level of single molecules in the gas-phase and in the implicit organic solvents chloroform and dichloromethane. The influence of the solvent environment was considered using the COSMO dielectric continuum model<sup>31</sup> with the default atomic cavity radii from Van der Waals radii obtained by Allinger et al.<sup>32</sup> divided by 1.2. The calculations adopted solvent radii of 3.17 Å for chloroform and 2.94 Å for dichloromethane with  $\text{cav0} = 0.0$  and  $\text{cav1} = 0.0067639$ . The starting structures of the molecules were obtained from the Cambridge Crystallographic Data Centre<sup>33</sup>. Geometric optimizations of the LS and HS structures were carried out using unrestricted PBE functional<sup>34</sup> and the Slater-type all-electron basis set TZP<sup>35</sup>, specifying the HS quintet state with four unpaired electrons, followed by the calculation of 303 harmonic vibrational frequencies for each geometry. For each material, 15 geometries were constructed by linearly interpolating between the optimized HS and LS geometries. Single-point energies for singlet, triplet, and quintet states of these geometries were calculated at the PBE/TZP level of theory in the unrestricted formalism. This approach is assumed to constitute the PESs of low-spin (LS;  $S=0$ ), intermediate spin (IS;  $S=1$ ), and high-spin (HS;  $S=2$ ) states.

At the cross geometry of the singlet and quintet state PESs, the excitation energies of the lowest three singlet states and three triplet states were calculated using the scalar relativistic effect of the zeroth-order regular approximation (ZORA)<sup>36,37</sup> formalism. The spin-orbit coupling constants ( $\zeta$ ) were derived, based on the one-electron spin-orbit coupling (SOC) integrals between the singlet and triplet states.

## Results and Discussions

### Free Energy Surfaces

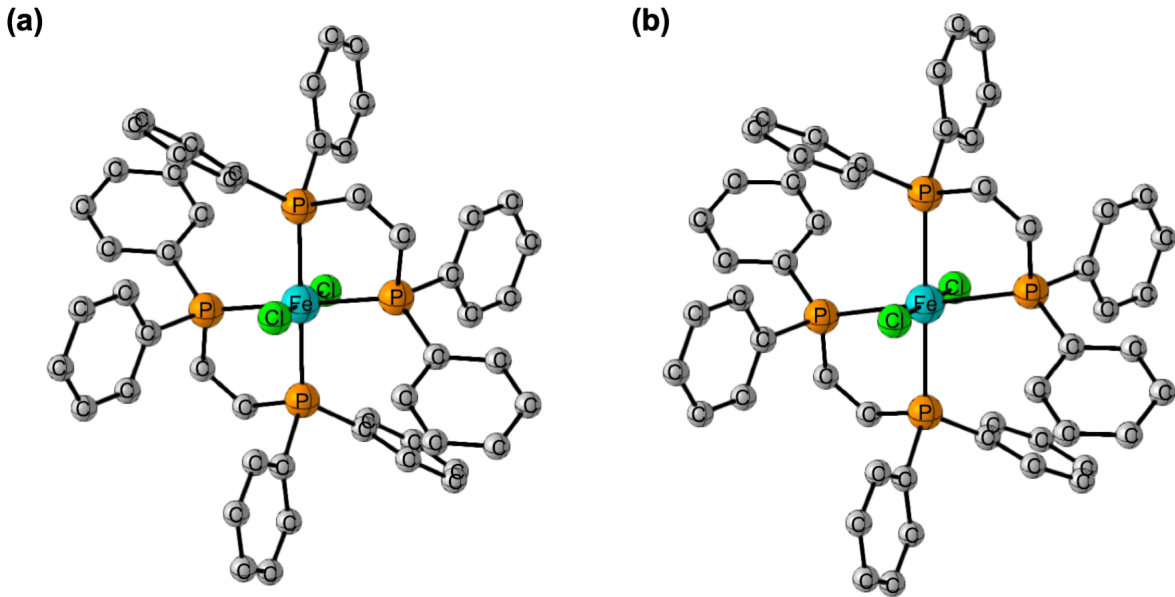


Figure 1: The optimised geometry of  $[\text{Fe}(\text{dppen})_2\text{Cl}_2]$  in LS state (a) and HS state (b) as obtained with UPBE/TZP. All hydrogen atoms are hidden for clarity.

We obtain the minimum energy geometries at the LS and HS states for the two complexes in three environments. Calculated coordination sphere bond lengths and distortion angles for all halogen and environment cases are given in the table 1. The table also labels each combination of halogen and environment with abbreviations that we use in the following discussion. The spin isomers display increases in the metal-ligand bond lengths from LS to HS structure in all environments. In all cases, the change is predominant in Fe-P bond

lengths,  $\Delta r_{\text{Fe-P}} \sim 0.29 \text{ \AA}$ . Whereas, Fe- $X$  bonds exhibit less significant changes ( $\sim 0.014 \text{ \AA}$  for  $X = \text{Br}$  and  $\sim 0.006 \text{ \AA}$  for  $\text{Cl}$ ). Compared to the gas phase, the solvent environments slightly reduce the change in Fe-P bonds by  $\sim 0.005 \text{ \AA}$  and also change Fe- $X$  bond length by  $\sim 0.009 \text{ \AA}$  accordingly. Changes in the M- $X$  bond lengths between the LS and HS states indicate a less significant involvement of these coordinates in SCO, compared to the M-P bonds. The optimized structures of all cases are given in the supplementary information.

Table 1: The values of average Fe- $X$  and Fe-P bond lengths differences between the HS and LS states, and angular distortion in both states  $\Sigma$  in the optimised DFT structures.

Complex	Solvent	Abbreviation	$\Delta r_{\text{Fe-X}}$ ( $\text{\AA}$ )	$\Delta r_{\text{Fe-P}}$ ( $\text{\AA}$ )	Angular distortion	
					$\Sigma_{\text{LS}}$ (deg)	$\Sigma_{\text{HS}}$ (deg)
[Fe(dppen) <sub>2</sub> Br <sub>2</sub> ]	vacuum	<b>1</b> Br <sub>2</sub>	0.008	0.293	76.4	86.7
[Fe(dppen) <sub>2</sub> Br <sub>2</sub> ]	CHCl <sub>3</sub>	<b>1</b> Br <sub>2</sub> (tcm)	0.014	0.288	76.2	89.6
[Fe(dppen) <sub>2</sub> Br <sub>2</sub> ]	CH <sub>2</sub> Cl <sub>2</sub>	<b>1</b> Br <sub>2</sub> (dcm)	0.021	0.287	76.2	90.1
[Fe(dppen) <sub>2</sub> Cl <sub>2</sub> ]	vacuum	<b>1</b> Cl <sub>2</sub>	0.001	0.299	75.1	85.1
[Fe(dppen) <sub>2</sub> Cl <sub>2</sub> ]	CHCl <sub>3</sub>	<b>1</b> Cl <sub>2</sub> (tcm)	0.009	0.294	74.4	85.6
[Fe(dppen) <sub>2</sub> Cl <sub>2</sub> ]	CH <sub>2</sub> Cl <sub>2</sub>	<b>1</b> Cl <sub>2</sub> (dcm)	0.010	0.293	74.2	85.7

In addition to the metal-ligand distances, angular distortions of the coordination environment in SCO complexes were suggested to play an important role in the dynamics<sup>38</sup>. Distortion from the perfect octahedral coordination sphere is measured as  $\Sigma = \sum_{i=1}^{12} |90^\circ - \phi_i|$ , where  $\phi_i$  is the angle between two metal-ligand bonds<sup>39</sup>. In all cases, The calculated HS structures have larger distortions compared to the LS structures, table 1. **1**Br<sub>2</sub> shows a small effect of the environment on the angular distortions, whereas **1**.Cl exhibits almost no environment effects. For **1**Br<sub>2</sub>(tcm), the optimized structural parameters of the inner coordination sphere from our DFT calculations are comparable to the experimental measurements on the solid-state [Fe(dppen)<sub>2</sub>Br<sub>2</sub>] · 2 CHCl<sub>3</sub><sup>9</sup> both in the LS and HS states, measured at 149 and 193 K respectively.

A comparison of the calculated energies of the LS and HS states is given in figure 2. X=Cl enhances the energy difference ( $\Delta E_{\text{HS-LS}}$ ) between the two spin states, as compared to Br. For example, the energy difference is 362 meV in **1**Br<sub>2</sub> and 412 meV in **1**Cl<sub>2</sub>. Solvation lowers  $\Delta E_{\text{HS-LS}}$  in all cases. In chloroform, the LS and HS state electronic energy difference

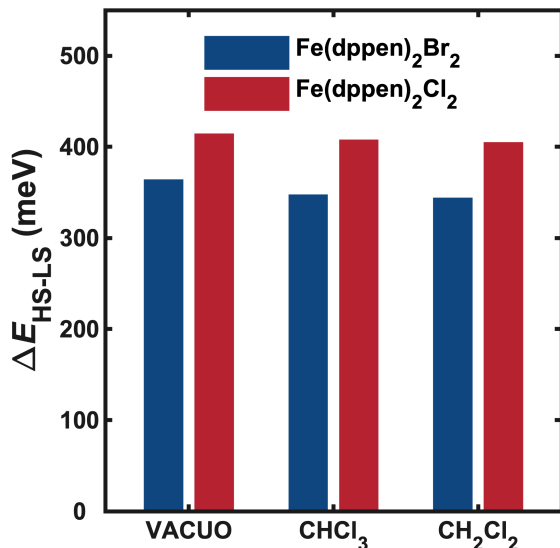


Figure 2: The electronic energy difference between HS and LS states,  $\Delta E_{\text{HS-LS}}$ , in different environments at UPBE/TZP level.

of **1**Br<sub>2</sub> and **1**Cl<sub>2</sub> reduces by 17 and 6 meV respectively. Whereas, the dichloromethane effect is stronger, where  $\Delta E_{\text{HS-LS}}$  reduces by 20 meV in **1**Br<sub>2</sub> and 9 meV in **1**Cl<sub>2</sub>.

Determining the spin crossover pathway on the full configuration space is computationally expensive, so we adopt a simpler approach. We define a coordinate  $q$  that linearly interpolates between the LS and HS state structures,  $q = 0$  and  $q = 1$  for the optimised LS and HS structures, respectively. The calculated LS and HS structures were used to construct 15 geometries on the reaction coordinate  $q = \{-0.2, -0.1, \dots, 1.1, 1.2\}$ . Figure 3 shows how the inner coordination sphere geometry varies along the interpolated path for **1**Cl<sub>2</sub>. By construction, the Fe-P and Fe-Cl bond lengths vary linearly with  $q$ , although the latter do not change significantly along this pathway. We find that the angular distortion also varies approximately linearly with  $q$ . Similar trends are found for all cases of halogens and solvents, figures S1-S5.

Next, we obtain diabatic potential energy surfaces (DPESs) along the reaction coordinate  $q$  of LS, HS and IS states. All DPESs were computed with unrestricted PBE/TZP. For all halogens and solvents, the IS state has a minimum at an intermediate value of the reaction

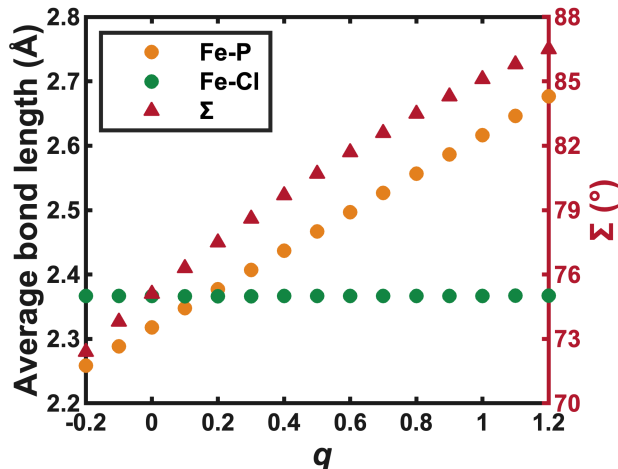


Figure 3: Variation of angular distortion ( $\Sigma$ ) and average metal-ligand bond lengths Fe-Cl and Fe-P with the reaction coordinate  $q$ , for  $1\text{Cl}_2$ .

coordinate,  $q \sim 0.3 - 0.4$ . For  $1\text{Cl}_2$ , PESs are plotted in figure 4. The calculated PESs for the other halogens and solvent are reproduced in figures S6-S10. Compared with the vacuum, energy gaps between the IS and low-energy LS and HS states are reduced by the solvents. In  $1\text{Cl}_2$ , the minimum energy crossing point (MECP) of LS and HS states is located at  $q_{\text{MECP}} = 0.6$ .  $q_{\text{MECP}}$  of all cases are listed in table 2, these are located at intermediate values of the angular distortions and bond lengths.

Direct transitions between the diabatic LS and HS states of figure 4a are spin-forbidden. Spin-orbit interaction allows intersystem crossings between the LS and IS states. Similarly, intersystem crossings are allowed between the HS and IS states. This gives a second-order spin-orbit interaction, which allows interconversion between the LS and HS states, mediated by at least one high-energy IS state.<sup>5,10</sup> We calculate the spin-orbit couplings between the spin-states, From DFT. Since the mixing between the LS and HS states is dominant near  $q_{\text{MECP}}$ , we consider  $q_{\text{MECP}}$  structures to determine the spin-orbit couplings between LS, IS and HS states.

Spin-orbit interaction is a single electron operator, thus the couplings between the many-electron spin-states can be parameterized with single electron integral  $\zeta$ <sup>40</sup>. LS-IS spin-orbit coupling is  $-\sqrt{6}\zeta$  and for HS-IS it is  $\sqrt{3}\zeta$ <sup>5,40</sup>. Table 2 summarizes  $q_{\text{MECP}}$  and  $\zeta$  values for

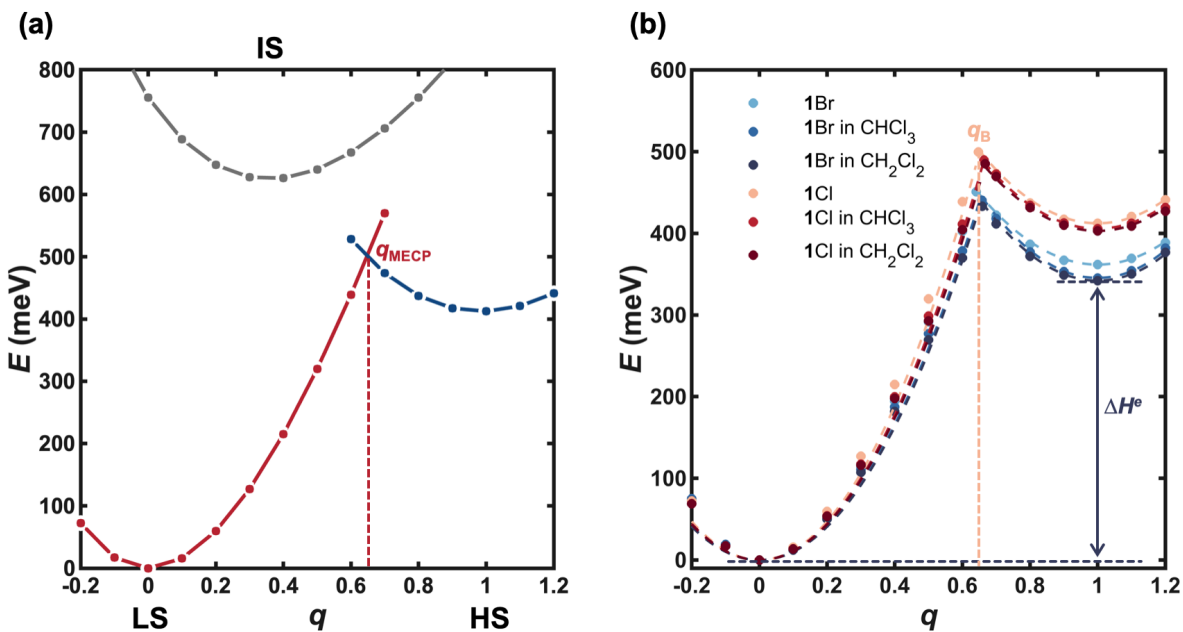


Figure 4: Ab-initio potential energies along the spin crossover reaction coordinate  $q$ . (a) Potential energy surfaces of  $1\text{Cl}_2$  in singlet (red), triplet (in grey) and quintet (blue) states. (b) The double-well (DW; solid) state is the potential energy surface only containing the low-spin to high-spin terms after mixing the low-spin, intermediate-spin, and high-spin states through spin-orbit interaction. The LS and HS parts (dashed curves) fit to the harmonic energy surfaces.

all cases. We find that Br enhances the spin-orbit coupling compared to Cl in the inner coordination sphere, a relativistic nephelauxetic effect due to heavier ligand<sup>41</sup>. Interestingly, the solvents decrease the magnitude of  $\zeta$  in the Br complex but increase it in the Cl complex. Thus, the choices of halogen in the ligand and solvents have highly nontrivial effects on the spin-orbit coupling.

Table 2: Calculated values of various parameters that determine SCO dynamics for all cases. Reaction coordinate  $q_{\text{MECP}}$  at MECP of LS and HS PESs, Spin-orbit coupling  $\zeta$ , electronic enthalpy difference between HS and LS states in the double well  $\Delta H^e$ , and force constants  $h_{\text{HS}}$  and  $h_{\text{LS}}$  for the two minima in the DW potential.

System	$q_{\text{MECP}}$	$\zeta$ (meV)	$\Delta H^e$ (eV)	Force constant	
				$h_{\text{LS}}$ (eV)	$h_{\text{HS}}$ (eV)
<b>1Br<sub>2</sub></b>	0.641	4.40 <i>i</i>	0.362	1.11	0.704
<b>1Br<sub>2</sub>(tcm)</b>	0.657	3.87 <i>i</i>	0.346	1.04	0.847
<b>1Br<sub>2</sub>(dcm)</b>	0.658	3.76 <i>i</i>	0.342	1.02	0.819
<b>1Cl<sub>2</sub></b>	0.647	2.32 <i>i</i>	0.412	1.18	0.728
<b>1Cl<sub>2</sub>(tcm)</b>	0.664	2.63 <i>i</i>	0.406	1.11	0.720
<b>1Cl<sub>2</sub>(dcm)</b>	0.667	2.64 <i>i</i>	0.403	1.09	0.708

Diagonalizing the DPESs, which are mixed due to the spin-orbit couplings, gives adiabatic potential energy surfaces (APESs) which are mixed LS, HS and IS along the reaction coordinate  $q$ . Note that we assume constant magnitudes of the spin-orbit at all  $q$  and obtained  $\zeta$  at the MECP geometries where the spin-orbit coupling has the largest effect. The lowest APES has two minima corresponding to LS and HS states, figure 4b shows the double well APES (DW-APES) of **1Cl<sub>2</sub>**. The DW-APES is at least pure LS at  $q = 0$  and at most HS state at  $q = 1$ . However, near the transition state—local maximum in DW-APES—the electronic state is a quantum superposition of the LS, HS and IS states.

To describe the SCO dynamics, we fit harmonic potentials to  $q = 0$  and  $q = 1$  minima of the DW-APES potential,

$$V_{\text{LS}} = h_{\text{LS}}q^2, \tag{1}$$

and

$$V_{\text{HS}} = h_{\text{HS}}(q - 1)^2 + \Delta H^e, \tag{2}$$

where  $h_{HS}$  and  $h_{LS}$  are the force constants at HS and LS minima respectively, and  $\Delta H^e$  is the electronic enthalpy difference of the two DW-APES minima, figure 4. The transition between the  $V_{LS}$  and  $V_{HS}$  is allowed at their crossing point. Figure 4b shows the fit for  $\mathbf{1Cl}_2$  to the DW-APES minima. Table 2 lists the fitting parameters used to for all cases.

In order to take into account the contribution of molecular vibrations to the enthalpy and entropy differences between the HS and LS states, we calculate the full vibrational spectra at the LS and HS geometries. Frequencies of 303 normal modes are obtained at the UPBE/TZP level in vacuo or considering the COSMO model (solvent = chloroform and dichloromethane). Calculated vibrational frequencies and intensities for all cases are given in the supplementary information, figures S11-S16.

The total enthalpy of each spin state depends on frequencies of all vibrational modes at a temperature<sup>42</sup>  $T$  is

$$H_{\Gamma}^{vib}(T) = \sum_{i=1}^{303} \hbar\omega_{i,\Gamma} \left( \frac{1}{2} + \frac{\exp(-\frac{\hbar\omega_{i,\Gamma}}{k_B T})}{1 - \exp(-\frac{\hbar\omega_{i,\Gamma}}{k_B T})} \right), \quad (3)$$

where  $\omega_{i,\Gamma}$  is harmonic frequency of  $i$ th mode in  $\Gamma$  spin state. Since the vibrational frequencies in the LS state are higher than the HS state, there is higher vibrational enthalpy in the LS state. The vibrational enthalpy difference between the HS and LS states  $\Delta H^{vib}(T) = H_{HS}^{vib}(T) - H_{LS}^{vib}(T) < 0$ . The plot of  $\Delta H^{vib}(T)$  for all cases is given in figure 5a. This difference decreases in magnitude at high temperatures, e.g., from  $\sim 11.9$  meV at 10 K to  $\sim 1.3$  meV at 610 K for  $\mathbf{1Br}_2$ . Solvents cause a small increase in the total enthalpy differences. Overall,  $\Delta H^{vib}(T)$  has following trend  $\mathbf{1Br}_2(\text{dcm}) > \mathbf{1Br}_2(\text{tcm}) > \mathbf{1Br}_2 > \mathbf{1Cl}_2(\text{tcm}) > \mathbf{1Cl}_2(\text{dcm}) > \mathbf{1Cl}_2$ .

The contribution of each harmonic oscillator to the total entropy depends on the frequencies of molecular modes and temperature<sup>42</sup>:

$$S_{\Gamma}(T) = \sum_{i=1}^{303} \left( \frac{\hbar\omega_{i,\Gamma}}{2T \tanh(\frac{\hbar\omega_{i,\Gamma}}{2k_B T})} - k_B \ln \left[ 2 \sinh\left(\frac{\hbar\omega_{i,\Gamma}}{2k_B T}\right) \right] \right). \quad (4)$$

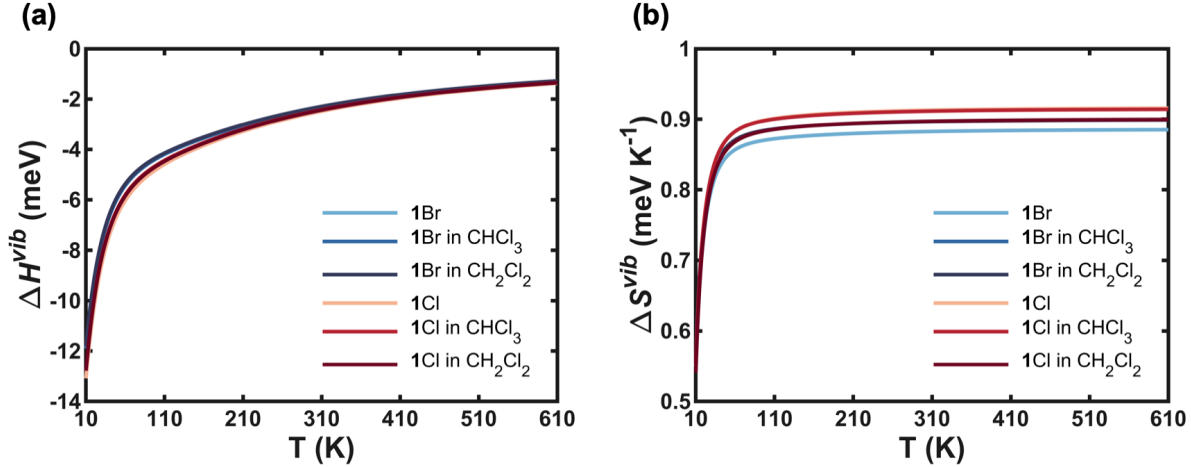


Figure 5: Calculated temperature-dependent vibrational enthalpy (a) and entropy (b) differences between the LS and HS states for all cases.

The vibrational entropy difference between the HS and LS states,  $\Delta S^{vib}(T) = S_{\text{HS}}^{vib}(T) - S_{\text{LS}}^{vib}(T)$  increases with temperature, 5b. Our calculated values at high temperatures are  $\sim 0.9 \text{ meV K}^{-1}$ , comparable to experimental estimates<sup>43</sup> for other spin crossover complexes. At large temperatures,  $\Delta S^{vib}(T)$  has the following trend  $1\text{Cl}_2 > 1\text{Cl}_2(\text{tcm}) > 1\text{Cl}_2(\text{dcm}) > 1\text{Br}_2(\text{tcm}) > 1\text{Br}_2(\text{dcm}) > 1\text{Br}_2$ .

Since the entropy and zero point enthalpy differences between the LS and HS states only change the free energy differences between the two states. To account for this difference, we include these to the HS free energy and obtain diabatic free energy surfaces from equations 1 and 2 as

$$G_{\text{LS}} = V_{\text{LS}}, \quad (5)$$

and

$$G_{\text{HS}} = V_{\text{HS}} + \Delta H^{vib} - T (\Delta S^{vib} + \Delta S^e), \quad (6)$$

Fig 6a shows that the difference between the free energy minima of the LS and HS states ( $\Delta G = \Delta G_{\text{HS}}(q=0) - \Delta G_{\text{LS}}(q=1)$ ), for each case of the halogens and solvents. At high temperatures,  $> 300 \text{ K}$ ,  $\Delta G$  becomes negative, thus, favouring the HS state at thermal equilibrium. We apply the classical transition state theory on these free energy potentials

to investigate the SCO dynamics. Free energy barriers from LS to HS transition,  $G_B^{\text{HS} \rightarrow \text{LS}}$ , and from HS to LS transition,  $G_B^{\text{LS} \rightarrow \text{HS}}$ , are defined at the crossing  $q_B$  of these free energies, which are also temperature dependent. Fig 6b gives the free energy barriers, that vary with temperature, for each halogen and solvent.  $G_B^{\text{LS} \rightarrow \text{HS}}$  is large at low temperatures and decreases with  $T$ , whereas,  $G_B^{\text{HS} \rightarrow \text{LS}}$  increases with  $T$ .

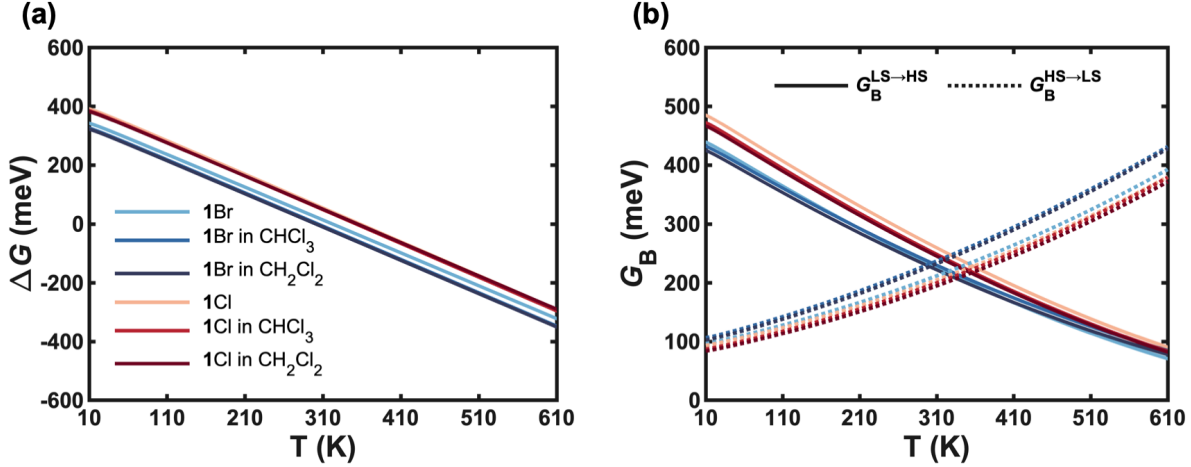


Figure 6: Calculated free energies and barriers for all halogens and environments. (a) Temperature-dependent free energy difference between the HS and LS states. (b) Temperature-dependent free energy barrier heights for the LS $\rightarrow$ HS and HS $\rightarrow$ LS dynamics.

## SCO Dynamics: Rates, $T_{\text{LIESST}}$ and $T_{1/2}$

We use the adiabatic free energies and the barriers, calculated above, to determine the spin crossover dynamics. Since the intermolecular interactions in solution are negligible, the SCO dynamics are governed by the single molecular theory<sup>44,45</sup>. At a temperature  $T$ , the classical transition rate<sup>46</sup> for a molecule to change from LS to HS is

$$k_{\text{LS} \rightarrow \text{HS}} = \sqrt{\frac{k_B T}{2\pi m_e (\Delta r_{\text{Fe-P}})^2}} \cdot \frac{\exp\left(-\frac{G_B^{\text{LS} \rightarrow \text{HS}}}{k_B T}\right)}{\int_{-\infty}^{q_B} \exp\left(-\frac{G_{\text{LS}}}{k_B T}\right) dq}. \quad (7)$$

Similarly,

$$k_{\text{HS}\rightarrow\text{LS}} = \sqrt{\frac{k_{\text{B}}T}{2\pi m_e(\Delta r_{\text{Fe-P}})^2}} \cdot \frac{\exp\left(-\frac{G_{\text{B}}^{\text{HS}\rightarrow\text{LS}}}{k_{\text{B}}T}\right)}{\int_{q_{\text{B}}}^{\infty} \exp\left(-\frac{G_{\text{HS}}}{k_{\text{B}}T}\right) dq}. \quad (8)$$

The kinetic energy,  $\propto k_{\text{B}}T$ , required for a process, e.g. HS $\rightarrow$ LS, is of the order of the relevant free energy barrier. At low temperatures,  $G_{\text{B}}^{\text{HS}\rightarrow\text{LS}} > G_{\text{B}}^{\text{LS}\rightarrow\text{HS}}$  for all halides and solvents, Fig 6b, hence  $k_{\text{HS}\rightarrow\text{LS}} < k_{\text{LS}\rightarrow\text{HS}}$  and the reverse is true at high temperatures.

We find that the combinations of halogens and solution environments significantly influence the SCO dynamics of phosphorene complexes. The temperature dependence of the calculated HS $\rightarrow$ LS relaxation rates is given in figure 7. Substituting Br anion in place of Cl in the inner coordination sphere slows HS $\rightarrow$ LS decay for all solution environments. This effect arises from the weaker ligand field from Br ion. Thus smaller electronic energy gap  $\Delta E_{\text{HS-LS}}$ , figure 2, in the complex **1Br**<sub>2</sub>, which gives larger free energy barrier compared to **1Cl**<sub>2</sub> in all environments.

However, mere energy gap consideration<sup>11</sup> does not fully explain the increase of relaxation rates due to the environment. Although, the solvents reduce the gap in both **1Br**<sub>2</sub> and **1Cl**<sub>2</sub>, **2**,  $k_{\text{HS}\rightarrow\text{LS}}$  do not generally decrease with solvents. For **1Cl**<sub>2</sub>, both solvents increase the rates, where the order of the rates is **1Cl**<sub>2</sub> < **1Cl**<sub>2</sub>(tcm) < **1Cl**<sub>2</sub>(dcm). For **X=Br**, both solvent lower the rates with order as **1Br**<sub>2</sub> < **1Br**<sub>2</sub>(dcm) < **1Br**<sub>2</sub>(tcm). For  $X=\text{Cl}$ , the energy gap decrease with solvents is not as sharp as for  $X=\text{Br}$  and the increase in the rates is defined by the free energy barriers, figure 6b. Spin-orbit interaction strength  $\zeta$  and the coordination sphere rigidity in the HS state defined by the constant  $h_{\text{HS}}$  significantly influence the transition state height in DW-APES, 4b and thus the barrier height. Larger  $h_{\text{HS}}$  give higher barrier and larger  $\zeta$  give smaller barrier heights.  $\zeta$  increasing with solvents, reducing the height of transition state, table 2, the order is **1Cl**<sub>2</sub> < **1Cl**<sub>2</sub>(tcm) < **1Cl**<sub>2</sub>(dcm). Stiffness of the coordination sphere in the HS state,  $h_{\text{HS}}$  decreases with solvents, reducing the height of transition state, table 2, order is **1Cl**<sub>2</sub> > **1Cl**<sub>2</sub>(tcm) > **1Cl**<sub>2</sub>(dcm). Thus overall effect of solvents is reduced transition state energy and faster HS $\rightarrow$ LS relaxations.

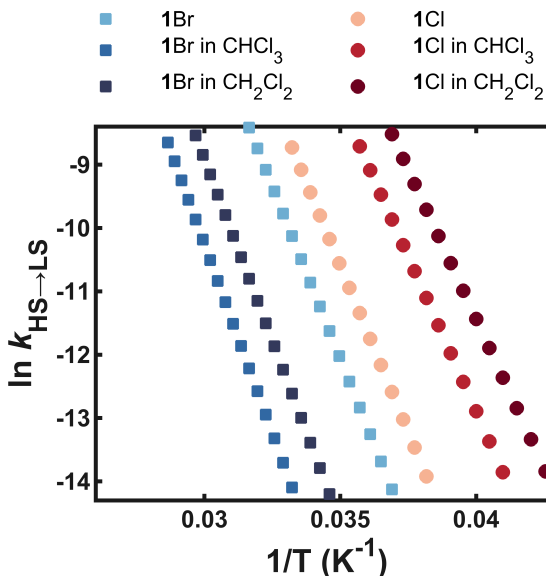


Figure 7: Calculated temperature-dependent relaxation rates of the HS to LS states.

Next, we calculate  $T_{\text{LIESST}}$  by warming the trapped HS state. Following the experimental protocol<sup>4</sup>, we heat the initial HS state from 10 K at  $0.3 \text{ K min}^{-1}$ . The population of LS and HS spin states are obtained from the rate equations based on  $k_{\text{HS} \rightarrow \text{LS}}$  and  $k_{\text{LS} \rightarrow \text{HS}}$ . The fractions of HS population  $\gamma_{\text{HS}}$  against temperature is plotted in figure 8a for all halogens and solvents.  $T_{\text{LIESST}}$ , defined as the minimum in  $\partial\gamma_{\text{HS}}/\partial T$ , is obtained from the kinetic data for each halogen and the solvent, table 3. In all environments,  $X=\text{Br}$  stabilizes the trapped HS state until higher temperatures than Cl. tcm and dcm solvents increase  $T_{\text{LIESST}}$  of Br compound, whereas decreases it in Cl complex.  $T_{\text{LIESST}}$  variations in the compounds primarily follow  $k_{\text{HS} \rightarrow \text{LS}}$ . The HS $\rightarrow$ LS kinetics predominate at these temperatures, as the thermal SCO, shown below, happens at much higher temperature.

The solvent effect is more pronounced in thermal spin-crossover in these compounds. To calculate  $T_{1/2}$ , we initialize in the all HS state at 610 K and cool at  $0.3 \text{ K min}^{-1}$ . The rate equations based on the calculated  $k_{\text{HS} \rightarrow \text{LS}}$  and  $k_{\text{LS} \rightarrow \text{HS}}$  determine the spin state population at each temperature step. Calculated values of  $T_{1/2}$  are given in table 3. Slow cooling rates do not change the calculated  $T_{1/2}$  values, supplementary information table S1. The environment effects  $T_{\text{LIESST}}$  just a few Kelvin, whereas Change in  $T_{1/2}$  due to the environment

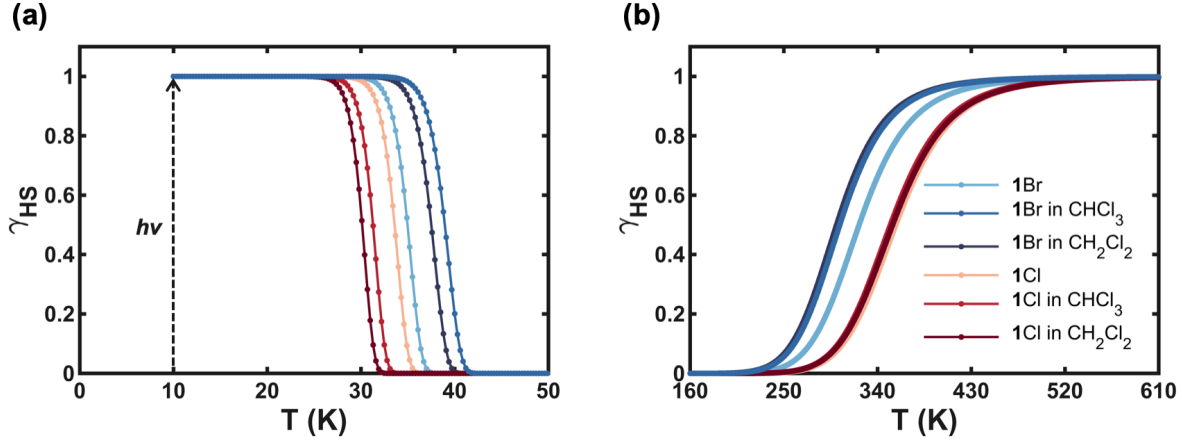


Figure 8: (a) Calculated thermally activated relaxation of the HS state initialized at 10 K. Kinetically trapped HS state is heated at a rate of  $0.3 \text{ K min}^{-1}$ .  $T_{\text{LIESST}}$  is obtained at the inflex points of the kinetic data for each case of Halogens and environments. (b) Calculated temperature dependence of HS fraction on heating the LS low-temperature state.

is significantly larger (10's of Kelvin). The thermodynamic relationship of the thermal SCO temperate  $T_{1/2} = \frac{\Delta E_{\text{HS-LS}}}{\Delta S_{\text{HS-LS}}(T_{1/2})}$  describes these calculated effects. The decrease in  $T_{1/2}$  for  $X=\text{Br}$  ( $\sim 22 \text{ K}$ ) is larger compared to  $X=\text{Cl}$  ( $\sim 5 \text{ K}$ ). In Br compounds, both  $\Delta E_{\text{HS-LS}}$  decrease and high temperature  $\Delta S_{\text{HS-LS}}^{\text{vib}}$  increase due to the solvents reduce  $T_{1/2}$ , figures 2 and 5. On the other for  $X=\text{Cl}$ , both  $\Delta E_{\text{HS-LS}}$  and  $\Delta S_{\text{HS-LS}}^{\text{vib}}$  decrease slightly, giving comparable  $T_{1/2}$  values.

Table 3: Calculated  $T_{\text{LIESST}}$  and  $T_{1/2}$  values, for two halogens and three environments. The experimental values of these compounds in solid solutions are also provided.

System	$T_{\text{LIESST}}$	$T_{1/2}$
1Br <sub>2</sub>	35.5	322.3
1Br <sub>2</sub> (tcm)	39.4	303.7
1Br <sub>2</sub> (dcm)	37.9	300.7
1Cl <sub>2</sub>	34.0	357.7
1Cl <sub>2</sub> (tcm)	31.6	352.3
1Cl <sub>2</sub> (dcm)	30.7	354.4

# CONCLUSION

From density functional theory, we have presented the SCO dynamics based on atomistic adiabatic free energy surface obtained from spin-orbit interaction induced superposition of LS, HS and IS state— a proof of concept using phosphorene based spin crossover complexes in solution. Comprehensive DFT calculations were performed for molecular structures, electronic states, spin-orbit coupling and vibrational frequencies to describe the temperature dependant SCO free energy surface.  $T_{\text{LIESST}}$  and  $T_{1/2}$  values are calculated from first principles, with varying halogen anions and solution environments.

Effects of halogen anions in the inner coordination sphere and solvents are elucidated. Replacing the Br with Cl anion in the inner coordination sphere increases the energy gap between the HS and LS states, reducing  $T_{1/2}$  and increasing  $T_{\text{LIESST}}$  values of  $\mathbf{1Br}_2$  in solvents dcm and tcm. The solvents decrease the energy gap of  $\mathbf{1Br}_2$  and  $\mathbf{1Cl}_2$  relative to the gas phase. However, the effect of solvents on  $T_{\text{LIESST}}$  and  $T_{1/2}$  values also depends on the halogen in the coordination sphere, table 3. For Br compounds,  $T_{\text{LIESST}}$  decrease and  $T_{1/2}$  increase with solvent. Whereas for Cl compounds, the solvents lower both  $T_{\text{LIESST}}$  and  $T_{1/2}$  values compared to the gas phase. The decrease in  $T_{\text{LIESST}}$  values of  $\mathbf{1Cl}_2$  in solution arise stronger spin-orbit coupling and weaker rigidity of inner coordination sphere, table 2.

The calculated trend of halogen substitution in  $\mathbf{1X}_2$ , Br lowers  $T_{1/2}$  and increases  $T_{\text{LIESST}}$  compared to Cl, was qualitatively observed, however, in the solid state samples.<sup>9</sup> However, care must be taken when comparing to experiments, our calculations only consider the complexes in solutions or vacuum and do not include solid-state effects which can significantly change the SCO properties, e.g., intermolecular interactions and guest molecules effects<sup>16</sup>. Moreover, a previous study has shown that the pure functional, such as PBE, overestimates the adiabatic high-spin and low-spin energy difference.<sup>47</sup> Employing a better exchange and correlation functional may improve the enthalpy difference calculations, such as the TPSSH functional with 10% exact exchange was suggested<sup>48</sup>.

## Acknowledgement

This work was supported by the Australian Research Council (DP230100139).

## Supporting Information Available

Additional results and optimized structure data are given in the supplementary information.

## References

- (1) Gütlich, P.; Gaspar, A. B.; Garcia, Y. Spin state switching in iron coordination compounds. *Beilstein Journal of Organic Chemistry* **2013**, *9*, 342–391.
- (2) Ksenofontov, V.; Levchenko, G.; Spiering, H.; Gütlich, P.; Létard, J.-F.; Bouhedja, Y.; Kahn, O. Spin crossover behavior under pressure of Fe(PM-L)<sub>2</sub>(NCS)<sub>2</sub> compounds with substituted 2'-pyridylmethylene 4-anilino ligands. *Chemical Physics Letters* **1998**, *294*, 545–553.
- (3) Zarembowitch, J.; Roux, C.; Boillot, M.-L.; Claude, R.; Itie, J.-P.; Polian, A.; Bolte, M. Temperature-, Pressure- and Light-Induced Electronic Spin Conversions in Transition Metal Complexes. *Molecular Crystals and Liquid Crystals Science and Technology. Section A. Molecular Crystals and Liquid Crystals* **1993**, *234*, 247–254.
- (4) Chastanet, G.; Desplanches, C.; Baldé, C.; Rosa, P.; Marchivie, M.; Guionneau, P. A critical review of the T(LIESST) temperature in spin crossover materials – What it is and what it is not. *Chemistry Squared* **2018**, *2*, 2.
- (5) Nadeem, M.; Cruddas, J.; Ruzzi, G.; Powell, B. J. Toward High-Temperature Light-Induced Spin-State Trapping in Spin-Crossover Materials: The Interplay of Collective and Molecular Effects. *Journal of the American Chemical Society* **2022**, *144*, 9138–9148.

- (6) Lefter, C.; Tan, R.; Dugay, J.; Tricard, S.; Molnár, G.; Salmon, L.; Carrey, J.; Nicolazzi, W.; Rotaru, A.; Bousseksou, A. Unidirectional electric field-induced spin-state switching in spin crossover based microelectronic devices. *Chemical Physics Letters* **2016**, *644*, 138–141.
- (7) Senthil Kumar, K.; Ruben, M. Emerging trends in spin crossover (SCO) based functional materials and devices. *Coordination Chemistry Reviews* **2017**, *346*, 176–205.
- (8) Díaz-Torres, R.; Chastanet, G.; Collet, E.; Trzop, E.; Harding, P.; Harding, D. J. Bidirectional photoswitchability in an iron (III) spin crossover complex: symmetry-breaking and solvent effects. *Chemical Science* **2023**, *14*, 7185–7191.
- (9) Wu, C.-C.; Jung, J.; Gantzel, P. K.; Gütlich, P.; Hendrickson, D. N. LIESST Effect Studies of Iron(II) Spin-Crossover Complexes with Phosphine Ligands: Relaxation Kinetics and Effects of Solvent Molecules. *Inorganic Chemistry* **1997**, *36*, 5339–5347.
- (10) Buhks, E.; Navon, G.; Bixon, M.; Jortner, J. Spin conversion processes in solutions. *Journal of the American Chemical Society* **1980**, *102*, 2918–2923.
- (11) Hauser, A. Intersystem crossing in Fe (II) coordination compounds. *Coordination Chemistry Reviews* **1991**, *111*, 275–290.
- (12) Wajnflasz, J. Etude de la transition "Low Spin"- "High Spin" dans les complexes octaédriques d'ion de transition. *physica status solidi (b)* **1970**, *40*, 537–545.
- (13) Boukheddaden, K.; Shteto, I.; Hôo, B.; Varret, F. Dynamical model for spin-crossover solids. I. Relaxation effects in the mean-field approach. *Physical Review B* **2000**, *62*, 14796.
- (14) Pavlik, J.; Linares, J. Microscopic models of spin crossover. *Comptes Rendus. Chimie* **2018**, *21*, 1170–1178.

- (15) Nishino, M.; Boukheddaden, K.; Konishi, Y.; Miyashita, S. Simple Two-Dimensional Model for the Elastic Origin of Cooperativity among Spin States of Spin-Crossover Complexes. *Physical review letters* **2007**, *98*, 247203.
- (16) Cruddas, J.; Powell, B. J. Structure–property relationships and the mechanisms of multistep transitions in spin crossover materials and frameworks. *Inorganic Chemistry Frontiers* **2020**, *7*, 4424–4437.
- (17) Ohlrich, M.; Powell, B. J. Fast, accurate enthalpy differences in spin crossover crystals from DFT+ U. *The Journal of Chemical Physics* **2020**, *153*.
- (18) Vela, S.; Fumanal, M.; Ribas-Arino, J.; Robert, V. Towards an accurate and computationally-efficient modelling of Fe (II)-based spin crossover materials. *Physical Chemistry Chemical Physics* **2015**, *17*, 16306–16314.
- (19) Vela, S.; Novoa, J. J.; Ribas-Arino, J. Insights into the crystal-packing effects on the spin crossover of [Fe II (1-bpp)] 2+-based materials. *Physical Chemistry Chemical Physics* **2014**, *16*, 27012–27024.
- (20) Bučko, T.; Hafner, J.; Lebègue, S.; Ángyán, J. G. Spin crossover transition of Fe (phen) 2 (NCS) 2: periodic dispersion-corrected density-functional study. *Physical Chemistry Chemical Physics* **2012**, *14*, 5389–5396.
- (21) Lebègue, S.; Pillet, S.; Ángyán, J. Modeling spin-crossover compounds by periodic DFT+ U approach. *Physical Review B—Condensed Matter and Materials Physics* **2008**, *78*, 024433.
- (22) Cirera, J.; Babin, V.; Paesani, F. Theoretical modeling of spin crossover in metal–organic frameworks:[Fe (pz) 2Pt (CN) 4] as a case study. *Inorganic Chemistry* **2014**, *53*, 11020–11028.

- (23) Cirera, J.; Ruiz, E. Computational modeling of transition temperatures in spin-crossover systems. *Comments on Inorganic Chemistry* **2019**, *39*, 216–241.
- (24) Vela, S.; Fumanal, M.; Sousa, C. Understanding kinetically controlled spin transitions in bistable spin crossover materials. *Journal of Materials Chemistry C* **2023**, *11*, 235–243.
- (25) Gütllich, P.; Goodwin, H. A. Spin crossover—an overall perspective. *Spin Crossover in Transition Metal Compounds I* **2004**, 1–47.
- (26) Chastanet, G.; Desplanches, C.; Baldé, C.; Rosa, P.; Marchivie, M.; Guionneau, P. A critical review of the T (LIESST) temperature in spin crossover materials- What it is and what it is not. *Chemistry Squared-Chem2* **2018**, *2*, 2.
- (27) Létard, J.-F.; Capes, L.; Chastanet, G.; Moliner, N.; Létard, S.; Real, J.-A.; Kahn, O. Critical temperature of the LIESST effect in iron(II) spin crossover compounds. *Chemical Physics Letters* **1999**, *313*, 115–120.
- (28) Marcén Murillo, S. Photomagnétisme de complexes du Fe(II) à ligandspolydentes. Enrichissement d'une base de données. Theses, Université Sciences et Technologies - Bordeaux I, 2003.
- (29) Hendrickson, D. N.; Adams, D. M.; Wu, C.-C.; Aubin, S. M. J. In *Magnetism: A Supramolecular Function*; Kahn, O., Ed.; Springer Netherlands: Dordrecht, 1996; pp 357–382.
- (30) te Velde, G.; Bickelhaupt, F. M.; Baerends, E. J.; Fonseca Guerra, C.; van Gisbergen, S. J. A.; Snijders, J. G.; Ziegler, T. Chemistry with ADF. *Journal of Computational Chemistry* **2001**, *22*, 931–967.
- (31) Pye, C. C.; Ziegler, T. An implementation of the conductor-like screening model of solvation within the Amsterdam density functional package. *Theoretical Chemistry Accounts* **1999**, *101*, 396–408.

- (32) Allinger, N. L.; Zhou, X.; Bergsma, J. Molecular mechanics parameters. *Journal of Molecular Structure: THEOCHEM* **1994**, *312*, 69–83.
- (33) Groom, C. R.; Bruno, I. J.; Lightfoot, M. P.; Ward, S. C. The Cambridge Structural Database. *Acta Crystallographica Section B* **2016**, *72*, 171–179.
- (34) Perdew, J. P.; Burke, K.; Ernzerhof, M. Generalized Gradient Approximation Made Simple. *Physical Review Letters* **1996**, *77*, 3865–3868.
- (35) Clementi, E.; Roetti, C. Roothaan-Hartree-Fock atomic wavefunctions: Basis functions and their coefficients for ground and certain excited states of neutral and ionized atoms,  $z \leq 54$ . *Atomic Data and Nuclear Data Tables* **1974**, *14*, 177–478.
- (36) Lenthe, E. v.; Baerends, E. J.; Snijders, J. G. Relativistic regular two-component Hamiltonians. *The Journal of Chemical Physics* **1993**, *99*, 4597–4610.
- (37) van Lenthe, E.; Baerends, E. J.; Snijders, J. G. Relativistic total energy using regular approximations. *The Journal of Chemical Physics* **1994**, *101*, 9783–9792.
- (38) Collet, E.; Guionneau, P. Structural analysis of spin-crossover materials: From molecules to materials. *Comptes Rendus Chimie* **2018**, *21*, 1133–1151.
- (39) Ketkaew, R.; Tantirungrotechai, Y.; Harding, P.; Chastanet, G.; Guionneau, P.; Marchivie, M.; Harding, D. J. OctaDist: a tool for calculating distortion parameters in spin crossover and coordination complexes. *Dalton Transactions* **2021**, *50*, 1086–1096.
- (40) Griffith, J. S. *The theory of transition-metal ions*; Cambridge university press, 1961.
- (41) Neese, F.; Solomon, E. I. Calculation of zero-field splittings, g-values, and the relativistic nephelauxetic effect in transition metal complexes. Application to high-spin ferric complexes. *Inorganic chemistry* **1998**, *37*, 6568–6582.
- (42) Bousseksou, A.; McGarvey, J. J.; Varret, F.; Real, J. A.; Tuchagues, J.-P.; Dennis, A. C.; Boillot, M. L. Raman spectroscopy of the high- and low-spin states of the spin

- crossover complex Fe(phen)<sub>2</sub>(NCS)<sub>2</sub>: an initial approach to estimation of vibrational contributions to the associated entropy change. *Chemical Physics Letters* **2000**, *318*, 409–416.
- (43) Sorai, M. Calorimetric Investigations of Phase Transitions Occurring in Molecule-Based Materials in Which Electrons Are Directly Involved. *Bulletin of the Chemical Society of Japan* **2002**, *74*, 2223–2253.
- (44) Hauser, A. Intersystem crossing in Fe(II) coordination compounds. *Coordination Chemistry Reviews* **1991**, *111*, 275–290.
- (45) Nadeem, M.; Powell, B. Theory of the Relaxation of Trapped Spin-States in Spin Crossover Materials: Drosophila for Complex Dynamics. **2023**,
- (46) Nitzan, A. *Chemical dynamics in condensed phases : relaxation, transfer and reactions in condensed molecular systems*; Oxford graduate texts; Oxford University Press: Oxford ;, 2006.
- (47) Song, S.; Kim, M.-C.; Sim, E.; Benali, A.; Heinonen, O.; Burke, K. Benchmarks and Reliable DFT Results for Spin Gaps of Small Ligand Fe(II) Complexes. *Journal of Chemical Theory and Computation* **2018**, *14*, 2304–2311.
- (48) Jensen, K. P.; Cirera, J. Accurate Computed Enthalpies of Spin Crossover in Iron and Cobalt Complexes. *The Journal of Physical Chemistry A* **2009**, *113*, 10033–10039.